

Journal of
Applied Remote Sensing

**Citrus greening disease detection using
aerial hyperspectral and multispectral
imaging techniques**

Arun Kumar
Won Suk Lee
Reza J. Ehsani
L. Gene Albrigo
Chenghai Yang
Robert L. Mangan

Citrus greening disease detection using aerial hyperspectral and multispectral imaging techniques

Arun Kumar,^a Won Suk Lee,^b Reza J. Ehsani,^c L. Gene Albrigo,^d
Chenghai Yang,^e and Robert L. Mangan^e

^aUniversity of Florida, Electrical and Computer Engineering, Gainesville, Florida 32611

^bUniversity of Florida, Agricultural and Biological Engineering, Gainesville, Florida 32611
wslee@ufl.edu

^cUniversity of Florida, Agricultural and Biological Engineering, Citrus Research and Education Center, Lake Alfred, Florida 33850

^dUniversity of Florida, Horticulture, Citrus Research and Education Center, Lake Alfred, Florida 33850

^eUSDA-ARS Kika de la Garza Subtropical Agricultural Research Center, Weslaco, Texas 78596

Abstract. Airborne multispectral and hyperspectral imaging can be used to detect potentially diseased trees rapidly over a large area using unique spectral signatures. Ground inspection and management can be focused on these detected zones, rather than an entire grove, making it less labor-intensive and time-consuming. We propose a method to detect the areas of citrus groves infected with citrus greening disease [Huanglongbing (HLB)] using airborne hyperspectral and multispectral imaging. This would prevent further spread of infection with efficient management plans of infected areas. Two sets of hyperspectral images were acquired in 2007 and 2009, from different citrus groves in Florida. Multispectral images were acquired only in 2009. A comprehensive ground truthing based on ground measurements and visual check of the citrus trees was used for validating the results using 2007 images. In 2009, a more accurate polymerase chain reaction test for selected trees from ground truthing was carried out. With a handheld spectrometer, ground spectral measurements were obtained along with their degrees of infection. A hyperspectral imaging software (ENVI, ITT VIS) was used for the analysis. HLB infected areas were identified using image-derived spectral library, mixture tuned matched filtering (MTMF), spectral angle mapping (SAM), and linear spectral unmixing. The accuracy of the MTMF method was greater than the other methods. The accuracy of SAM using multispectral images (87%) was comparable to the results of the MTMF and also yielded higher accuracy when compared to SAM analysis on hyperspectral images. A possible inaccurate ground truthing for the grove in 2007 generated more false positives. © 2012 Society of Photo-Optical Instrumentation Engineers (SPIE). [DOI: [10.1117/1.JRS.6.063542](https://doi.org/10.1117/1.JRS.6.063542)]

Keywords: Huanglongbing; linear spectral unmixing; mixture tuned matched filtering; spectral angle mapping.

Paper 11001 received Jan. 1, 2011; revised manuscript received Apr. 26, 2012; accepted for publication Apr. 30, 2012; published online Jun. 1, 2012.

1 Introduction

Citrus greening, also called Huanglongbing (HLB) or yellow dragon disease, is thought to have originated from China in the early 1900s. The disease is primarily spread by two species of psyllid insects. The disease in Florida is caused by a bacterium, *Candidatus Liberibacter asiaticus*,¹ that is transmitted by a tiny insect, the Asian citrus psyllid (*Diaphorina citri*), which thrives on young citrus leaves. The Asian citrus psyllid has been present in Florida since 1998.² There are three strains of the bacteria: an Asian version, an African version, and an American strain discovered in Brazil. The Asian strain, *Candidatus Liberibacter asiaticus*,

was found in Florida in early September 2005. The bacteria itself is not harmful to humans, but the disease has harmed trees in Asia, Africa, the Arabian Peninsula, and Brazil.³

HLB is one of the world's most destructive and devastating citrus diseases. The HLB infected trees die within three to five years and produce fruits which are unmarketable once the disease obstructs the flow of nutrients in citrus trees. Since no cure is known, the infected trees have to be removed and destroyed. HLB has now emerged as the major threat to the Florida's \$9 billion citrus industry. As of February 2010, citrus trees in 3122 different sections (square mile) in 34 counties were infected in Florida.⁴ Growers urgently need diagnostic tools for early detection, because infected trees may not show symptoms for months or years, during which they are contagious. Current molecular diagnostic tests do not detect the disease soon enough to stop its spread. These methods proved inadequate, and many growers are not replanting, because young, vigorous trees attract psyllids. As the bacteria moves within the tree, the entire canopy progressively develops a yellow color as shown in Fig. 1. The most characteristic symptoms of citrus greening are a blotchy leaf mottle and vein yellowing that develop on leaves attached to shoots showing the overall yellow appearance. On Mandarin oranges, fruit may develop an uneven ripening such that they appear half orange and half green on the shaded side. This symptom is the origin of the common name "greening."

Culturing and sequencing the genome of the greening pathogen and the host would facilitate studies of interactions between the host, the bacteria, and the insect that acts as a carrier or vector of the disease.⁵ This would aid in development of diagnostic tools that would enable early detection of infected trees. Until such tools are available, we need to find ways by which we can detect HLB infected areas within citrus groves and monitor newly infected areas. A polymerase chain reaction (PCR) method can be used to confirm infections of HLB, but the process is expensive and hence not feasible and economical for larger areas. Moreover, time-consuming and labor-intensive ground-based inspection methods are not suitable for identifying all individual tree infections over a larger area.

Hyperspectral imaging can provide unique spectral signatures and thus can be used to detect potentially infected trees over a large area for rapid detection of infected zones, where ground inspection and management should be focused. This will significantly reduce the cost of surveying, allow for monitoring new areas, and provide faster results. Morris and Muraro⁶ reported that the average cost for ground scouting for the citrus greening disease was \$90/ac per year in the 2008 to 2009 season in Florida.

Hyperspectral reflectance imaging has been successfully used to identify disease, deficiencies, and defects in different fruits and vegetables. As an example of a citrus disease detection, a spectral information divergence-based image classification method provided useful means for detecting canker lesions on citrus fruit.⁷ In this study, a significant problem was that greasy spot, insect damage, and melanose had similar reflectance properties to canker, and the chances for misclassifying these three diseases were higher than other kinds of peel conditions. Hyperspectral imaging has been used to detect disease for other crops such as rice and lettuce. Rice canopy hyperspectral reflectance has been used to detect bacterial leaf blight (BLB) by establishing spectral models for



Fig. 1 An Huanglongbing infected citrus tree.

assessing disease severity for future site-specific management.⁸ Hyperspectral images in the range from 339 to 1014 nm have been used to detect disease during early stages of lettuce growth.⁹ It has been observed that plants under stress induced by a disease, based on the severity of the infection, tend to absorb more light in the near infrared (NIR) spectrum. For fruit defect detection, the reflectance spectra from the hyperspectral images of apples have been used to find the optimal wavelengths to discriminate the defective region from the normal region.¹⁰

The overall objective of this study is to develop a method to detect HLB infected areas in citrus groves using airborne hyperspectral and multispectral imaging which will enable more rapid detection of potentially infected areas. This, coupled with development of efficient management plans of these areas, will therefore prevent further spread of the infection.

2 Citrus Grove Site, In-Field Measurements and Ground Truthing

Airborne imagery was acquired twice, once in 2007 and another in 2009, from two different locations, which are described below. In 2007, only hyperspectral images were taken, while hyperspectral and multispectral images were taken in 2009.

2.1 Citrus Grove Site: 2007

The citrus grove chosen for this study in 2007 was located in the southern part of Hendry County in Florida, USA, and spread across 800 hectares (~1.6 km wide and 5.0 km long). The center coordinates of this location are 26°23' 21.41"N and 80°57' 25.06"W. Ground truthing revealed that the grove had about 10,000 HLB infected trees and hence made it a suitable candidate for this study. The ground truthing was based on visual check and done by recording locations of infected trees using a differential Global Positioning System (DGPS) receiver. The grove contained Valencia and Hamlin oranges.

Reflectance data from ground measurements were obtained for infected and healthy citrus trees using a portable spectrometer (Fieldspec, ASD Inc.). A total of 21 different measurements were obtained for both infected and healthy trees. Degree of infection (HLB1, HLB2, or HLB3) was mentioned in each recording from the infected trees where HLB1 indicated least infection and HLB3 indicated the highest level of infection. The ground spectrometer recordings spanned across 350 to 2500 nm with a 3 nm spectral resolution.

2.2 Citrus Grove Site: 2009

The citrus grove chosen for this study in 2009 was located in Collier County in Florida, USA, and was spread across 77.37 acres. The center coordinates of this location were 26°21' 12.27"N and 81°21' 15.76"W. A multispectral and a hyperspectral image were acquired from both blocks marked E1 in Fig. 2. The grove contained Valencia oranges.

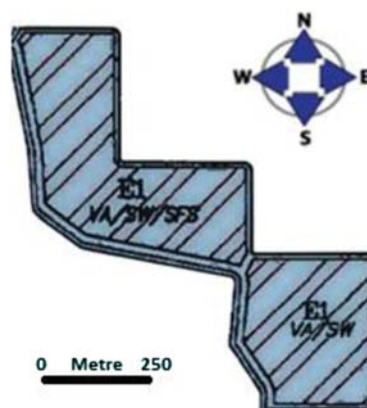


Fig. 2 Citrus grove site under study (Summerland Grove–Consolidated Citrus Limited Partnership).

In-field measurements were obtained from the study site using a portable handheld spectrometer (HR-1024, Spectra Vista Corporation, Poughkeepsie, New York) for four different categories of trees in the grove. The categories were HLB1 (tree canopy infected in some parts), HLB2 (HLB infected tree in general decline), nutrient deficient (but no HLB infection), and healthy tree. In 2009, different class definitions were used, since the tree conditions were different than in 2007. The ground spectrometer recordings spanned across 348 to 2300 nm with a 3 nm spectral resolution.

The PCR-based ground truthing for confirming HLB infection was conducted for selected trees in the study site. The ground truthing was carried out by recording locations of infected trees using a real-time kinematic (RTK) GPS receiver (HiPer XT, Topcon, Olathe, KS).

3 Airborne Imaging System

3.1 Hyperspectral Imaging System for Images Taken in 2007

Hyperspectral images were obtained using an airborne hyperspectral camera (AISA Eagle, Spectral Imaging Ltd., Finland) which was incorporated with a GPS/inertial measurement unit (IMU). This push broom sensor acquired imagery over a spectral range of 397.3 to 995.3 nm with 128 bands at an altitude of 1158 m. The spectral resolution was approximately 5 nm, and the spatial resolution of the imagery was 0.7 m.

All data were radiometrically calibrated to radiance data based on the following steps. First, the sensor noise was removed by subtracting the mean value of every flight line of the dark data from the corresponding flight line of the raw data. A separate dark image was acquired for every raw image (flight line). Then the raw data were calibrated to radiance units using a calibration file, which was supplied by the manufacturer of the camera (SPECIM). Every spatial and spectral pixel was multiplied with the corresponding value in the calibration file. The values for each pixel on the CCD were calculated using an integrating sphere. Then the smile effect (changes in wavelength over the field of view) was corrected. The radiance unit was equal to $\text{mW}/\text{cm}^2 \cdot \text{sr} \cdot \mu\text{m}$. The digital number (DN) in the radiance file had a scale of 1000. The individual radiance files were grouped to form mosaic files of different regions. The radiance image files were converted to reflectance, which accounts for changes in irradiance over time and for solar position, solar zenith angle, and Sun-Earth distance. The FLAASH model atmospheric correction method in the hyperspectral imaging software package (ENVI 4.6, ITT VSI, Boulder, Colorado, USA) was used for this conversion.

The calibrated data were then geo-referenced using the Shuttle Radar Topography Mission (SRTM) elevation data using ENVI. The final mosaic images were presented in UTM zone 17N projection with the datum of World Geodetic System (WGS) 84. The accuracy was estimated to be approximately one to two pixels.

3.2 Hyperspectral and Multispectral Imaging System for Images Taken in 2009

A high-resolution airborne four-camera imaging system¹¹ and a hyperspectral imaging system¹² were used for image acquisition in 2009. The multispectral system (XMV-4021 CCD camera, Illunis LLC, Minnetonka, MN) acquired 12-bit images with 2048×2048 pixels in blue (430 to 470 nm), green (530 to 570 nm), red (630 to 670 nm), and NIR (810 to 850 nm) bands.

The CCD-based hyperspectral sensor captured 128-band images covering a spectral range from 457.2 to 921.7 nm at 3.63 nm intervals. The image swath was 640 pixels, and the radiometric resolution was 12 bits.

The multispectral image was acquired at an altitude of 3048 m, while the hyperspectral image was acquired at 1524 m. Both images were georeferenced to the Universal Transverse Mercator (UTM) coordinate system with zone 17N projection with the datum of WGS-84 and resampled to 1 m pixel resolution, which was the pixel size of the geo-referenced RGB image. The images were not radiometrically calibrated, and the DNs on the imagery were represented using 12-bit numbers, ranging from 0 to 4095. The specifications of the imaging systems used are summarized in Table 1.

Table 1 Specifications of the various imaging systems used.

Specification	AISA Eagle	Hyperspectral camera	Multispectral camera
Sensor type	Progressive scan CCD camera	CCD-interline progressive scan	CCD-interline progressive scan
Sensing area (mm)	12.29	8.6 × 6.9	15.2 × 15.2
Pixel size (μm)	12	6.7 × 6.7	7.4 × 7.4
Active pixels ($h \times v$)	1024	1280 × 1024	2048 × 2048
Pixel depth	12 bit	12 bit	12 bit
Spectral range (nm)	397 – 955	457 – 922	400 – 1000
Spectral resolution (nm)	4.7	3.6	N/A
Spatial resolution (m)	0.7	1.0	0.5
Center wavelength	N/A	N/A	480 nm (blue), 560 nm (green), 650 nm (red), 830 nm (NIR), with 10 nm FWHM
Number of spectral bands	128	128	4
Altitude (m)	1158	1524	3048

4 Methods

4.1 Spectral Library Construction from 2007 Images: Reflectance Data

ENVI 4.6 was used for the collection of reflectance data from the pixels of the hyperspectral images. The mosaic image of the selected grove site for the study was split into 12 blocks (approximately 60 hectare each), and each block was further divided into 13 sections of 100,000 pixels each. Eight sections within the entire collection of sections were identified as young trees (shorter trees compared to the rest of the sections). All other sections were classified into the large tree category (having wider canopy spread).

A total of 52 sections were created which were divided randomly into training (70% or 37 sections) and validation (30% or 15 sections) data sets. The ground truth information for the site was used as reference for collecting pixels for building the spectral library. A set of pixels from the training set was collected for each of the 10 classes shown in Table 2. A count of 90 pixels was collected for each of the major tree pixel classes ('HLB' and 'Healthy') and 20 pixels each for the rest of the categories.

4.2 Spectral Library Construction from 2009 Images: Uncalibrated Data

Pixel spectra were collected from both the hyperspectral and the multispectral image corresponding to the locations recorded for each of the categories mentioned in the in-field ground measurements. The pixel spectra for each tree flagged under various categories in the ground measurement were collected, and there were a total of 49 observations for HLB1 class, 20 observations for HLB2 class, 24 nutrient deficient, and 11 healthy tree spectra.

Pixel spectra were collected for the trees which were confirmed HLB positive and those declared healthy based on the PCR results. Using the PCR tests, a total of 30 HLB infected trees were identified, and their corresponding pixel spectra were collected from the hyperspectral and multispectral image. A total of 20 infected pixel spectra, 10 pixels each from both the E1 blocks of the citrus grove, formed a training set of the image derived spectral library. The remaining 10 pixels formed a validation set of spectral library against which detection accuracy of the image analysis would be documented.

Table 2 Ten different classes used in this study and their description.

Class	Description
HLB	HLB infected canopy in the row center
HLB_L	HLB infected canopy in the west side of a row
HLB_R	HLB infected canopy in the east side of a row
Healthy	Healthy canopy in the row center
Healthy_L	Healthy canopy in the west side of a row
Healthy_R	Healthy canopy in the east side of a row
HLB_LY	HLB infected canopy of younger trees in the west side of a row
HLB_RY	HLB infected canopy of younger trees in the east side of a row
Healthy_LY	Healthy canopy of younger trees in the west side of a row
Healthy_RY	Healthy canopy of younger trees in the west side of a row

4.3 Reflectance Data Analysis: 2007 Images

Discriminant analysis was conducted to determine the strength and validity of the classification. Analysis of variance (ANOVA) using SAS was carried out to extract the significant spectral bands at which the healthy and diseased pixels could be separated for all categories. The section images in the training set were used to obtain necessary parameters such as NDVI (normalized difference vegetation index)¹³ threshold. NDVI was used to eliminate the nonvegetation pixels from the images in the training set, which subsequently was used for the spectral angle mapping (SAM).¹⁴ SAM was carried out on a few randomly selected images from the training set using the spectral subset extracted using ANOVA. The accuracy of results from HLB identification using SAM analysis was recorded against the ground truth vectors on a pixel match basis.

False positives (healthy trees identified as infected) were a major concern in the results obtained from this image analysis. A false positive pixel library of 30 samples was built from the validation set using the image results obtained from the SAM image analysis. ANOVA was carried out on the reflectance data obtained from the false positive samples and HLB pixel collection in order to extract spectral bands which could separate the two categories. The objective for this procedure was to use these spectral bands for image analysis and observe its effect on the results obtained. Moreover, the results were validated against a tree-based visual check approach instead of a pixel-based approach. Each large tree canopy usually formed a 4×4 pixel matrix which can be differentiated from each other by a zoom in visual check.

Various vegetation indices (VIs) and leaf pigment indices were calculated for Healthy and HLB categories using the reflectance data from ground measurements. The same was calculated for the data from the image derived spectral library and validated against the results from the ground data. VIs such as the Red Edge Normalized Difference Vegetation Index (RENDVI),¹⁵ Atmospheric Resistant Vegetation Index (ARVI),¹⁶ and leaf pigment indices such as the carotenoid reflectance index and anthocyanin reflectance index were used for this study. These are summarized in Table 3.

The RENDVI ($NDVI_{705}$) is a modification of the traditional broadband NDVI. It was chosen since it is intended for use with very high spectral resolution reflectance data, such as from hyperspectral sensors and for applications such as vegetation stress detection.¹⁷ This VI differs from the NDVI by using bands along the red edge, instead of the main absorption and reflectance peaks. The ARVI is enhancement to the NDVI that is relatively resistant to atmospheric factors and was more suitable for the aerial images in this study.

There are three main categories of leaf pigments in plants: chlorophyll, carotenoids, and anthocyanins. The carotenoid and anthocyanin pigments often appear in higher concentrations

Table 3 Vegetation indices used to reduce false positives.

Vegetation Index (VI)	VI Formula
Anthocyanin Reflectance Index (ARI)	$((1/\rho_{550}) - (1/\rho_{700}))$
Atmospheric Resistant Vegetation Index (ARVI)	$[(\rho_{NIR} - (2\rho_{RED} - \rho_{BLUE})) / (\rho_{NIR} + (2\rho_{RED} - \rho_{BLUE}))]$
Carotenoid Reflectance Index (CRI)	$(1/\rho_{510}) - (1/\rho_{550})$
Red Edge Normalized Difference Vegetation Index (RENDVI)	$(\rho_{750} - \rho_{705}) / (\rho_{750} + \rho_{705})$

in vegetation that is less healthy or undergoing stress such as in citrus trees affected with HLB. The VIs and leaf pigment indices were used to determine suitable threshold values for refining the pixel collection in the spectral library by eliminating pixels which would have found a place in the pixel collection due to inaccuracy in ground truthing. This method therefore establishes a workaround, even if the ground truth data is not accurate. ANOVA was carried out again for VI refined true HLB pixels and healthy pixels, in order to extract new significant bands for image analysis.

The identification of infected trees in the validation set was conducted using the spectral subset obtained from the significant bands, the image derived spectral library having significant band information, mixture tuned matched filtering (MTMF), and SAM tools in ENVI. Matlab (Mathworks) and SAS were used for the statistical data analysis.

4.4 Data Analysis and Pixel Detection: 2009 Images

A total of 20 infected pixel spectra from the spectral library, 10 pixels each from both E1 blocks of the grove, formed a training set of the image derived spectral library. The remaining 10 pixels formed a validation set against which detection accuracy of the image analysis would be documented. Endmember detection algorithms such as SAM, MTMF, and linear spectral unmixing (LSU) were applied on the hyperspectral and multispectral images.

5 Results and Discussion

In this section, five different detection methods for the HLB disease are presented. The procedure of each method is explained, and its results are presented and discussed. Since the status of every tree on the grove is not known, quantizing the false positives (healthy tree identified as infected) is not possible. This would have provided an even better representation and accuracy of the results.

5.1 Results from Analysis of Reflectance Data from 2007 Hyperspectral Images

Due to significant variations of pixel characteristics within the imagery, healthy and HLB infected pixels were further categorized. It was observed that pixels at the canopy edge had lower reflectance compared to the pixels at the center due to shadow and illumination differences. It was further observed that spectra obtained from the left canopy edge in the west side were different from those on the right edge in the east side due to illumination at 4 PM local time. Figure 3 shows the spectral profiles obtained from an average of 30 pixels collected for each of the tree pixel categories for large trees. The classes in young trees also followed a similar trend. It was observed that healthy and HLB classes can be clearly differentiated in the NIR region.

Spectral libraries of 90 pixels each, corresponding to each of the tree pixel endmember classes for the larger tree category, were built for further study. The same was repeated for the young tree category with 20 pixels from each of its classes. A discriminant analysis was carried out on the spectral library to observe how strongly the naturally occurring groups of healthy and HLB infected pixels can be classified and separated. The confusion matrix obtained as a result of the analysis is shown in Table 4. Error signifies the degree of misclassification of the pixels.

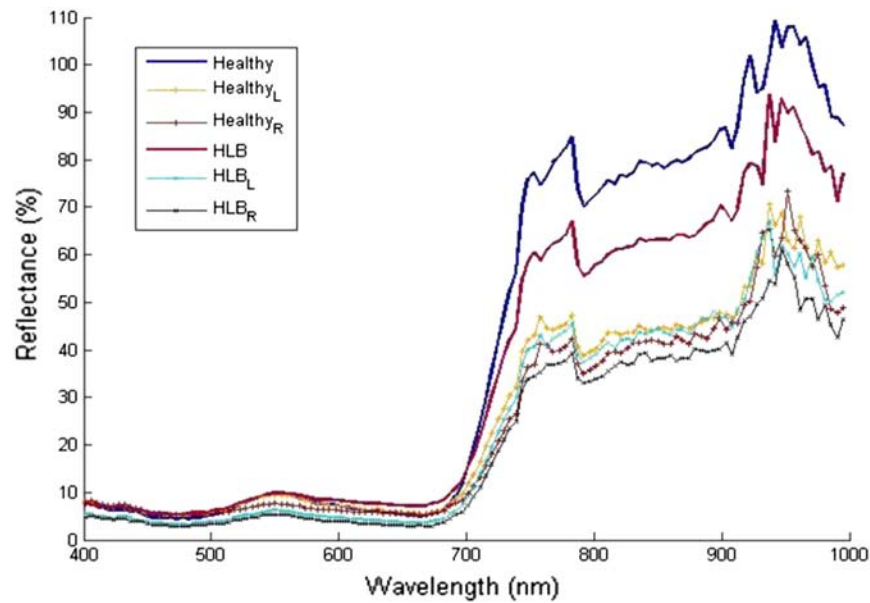


Fig. 3 Spectral plot of six different classes for the large-tree pixel category.

Table 4 Discriminant analysis on the spectral library, showing the number of pixels in each category.

		Healthy	HLB	Total	Error (%)
Large tree	Healthy	53	37	90	41.1
	HLB	26	64	90	28.9
Young tree	Healthy	14	6	20	30.0
	HLB	7	13	20	35.0

The confusion matrix indicated a significant amount of misclassification, and this was further confirmed by the occurrence of false positives during MTMF and SAM analyses. In order to extract the significant bands at which the healthy and diseased pixels could be separated for all categories, analysis of variance (ANOVA) was carried out on all pixel observations from the spectral library for both young and large trees. Those bands were selected which had a low p -value. A p -value lower than 0.05 was evidence against the null hypothesis and suggested that there was larger and more significant difference between the groups (Healthy and HLB infected) than within the same hyperspectral band for the observations. Forty-four significant bands were extracted for the large tree pixels and 36 bands for the young trees. The spectral bands identified for large trees were 734 to 927 nm, 975, and 980 nm. For the young trees, the spectral bands were 410 to 432 nm, 440 to 509 nm, 634 to 686 nm, 932, and 951 nm.

5.2 Results from Analysis of Reflectance Data from 2009 Site and Hyperspectral Images

The portable spectrometer readings for all the data points from the citrus grove site are plotted in Fig. 4, showing the difference in the spectral characteristics of the tree categories classified. The spectra for HLB1, HLB2, nutrient deficient, and healthy are the average of 49, 20, 24, and 11 spectral measurements, respectively. Both categories of HLB show higher reflectance in the visible region compared to both nutrient deficient and healthy trees. The data corresponding to the range of 1800 to 2000 nm were found to be noisy due to low signal levels due to water vapor absorption, and hence they were removed from the plot.

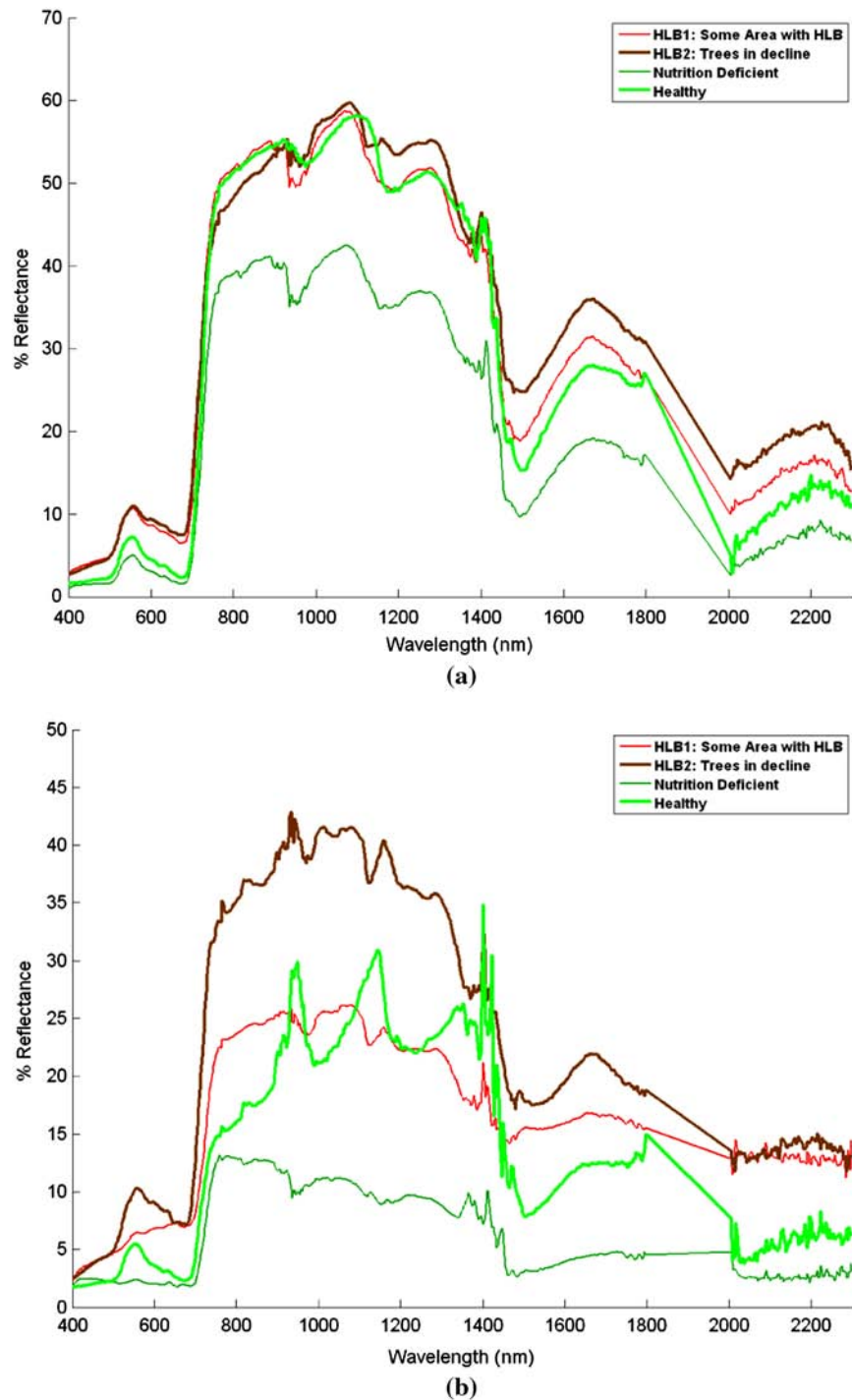


Fig. 4 Example of a spectral data analysis from ground measurements. A portable handheld spectrometer was used to measure in-field reflectance spectra of HLB infected (HLB1 and HLB2), nutrient deficient trees and healthy canopies. (a) The mean spectra for HLB1, HLB2, nutrient deficient, and healthy are the average of 49, 20, 24, and 11 spectral measurements, respectively. (b) Standard deviation of the measurements.

The trees used for ground measurements were marked on the hyperspectral and multispectral images. The corresponding pixel spectra of these data points from hyperspectral and multispectral images are shown in Fig. 5(a). It can be seen that the DN value for HLB1 is higher than the Healthy tree category in both the hyperspectral and multispectral images. This is consistent with spectral plot of in-field reflectance measurements.

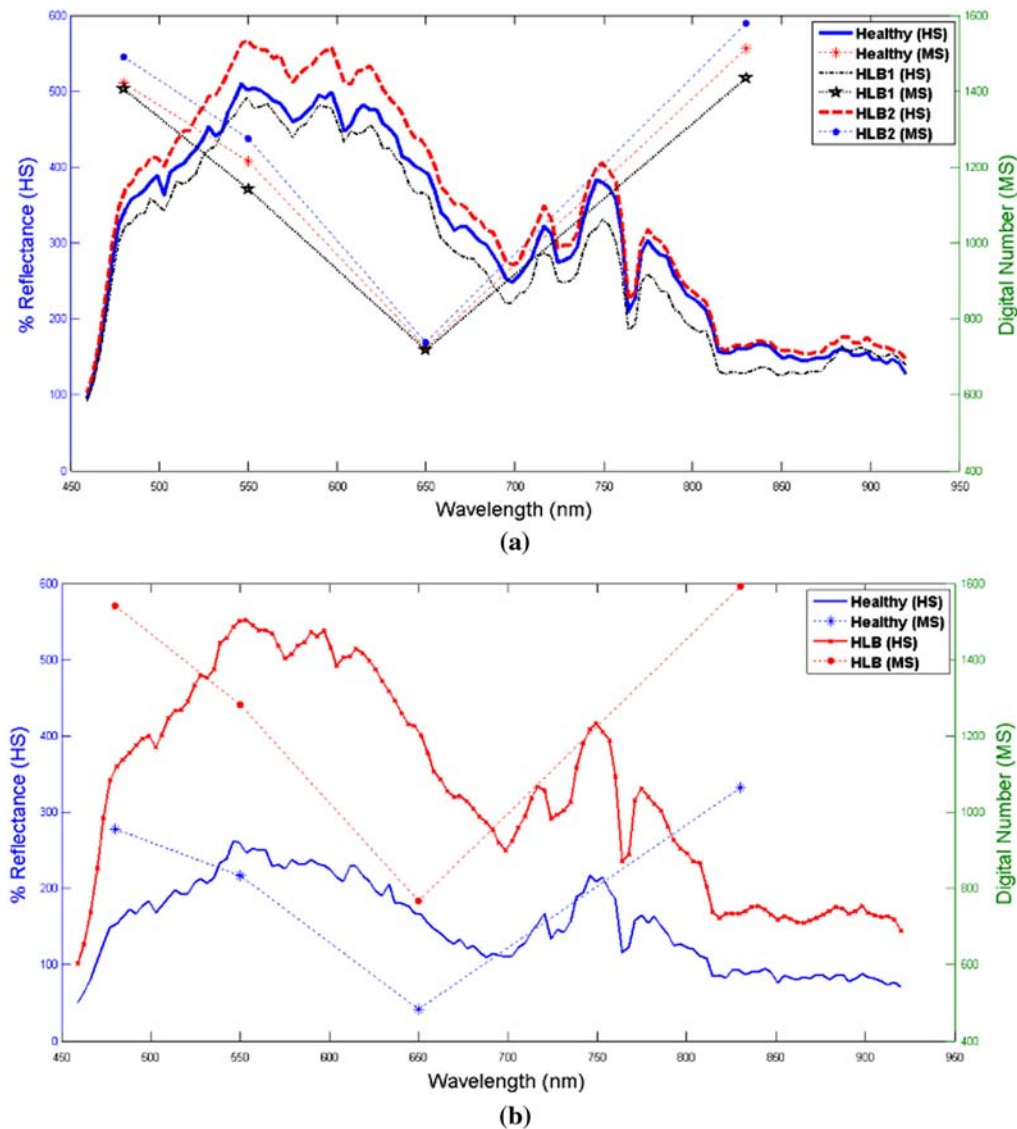


Fig. 5 Pixel data analysis from hyperspectral and multispectral images. (a) Spectral plot of HLB infected (HLB1 and HLB2) and healthy canopies corresponding to trees in ground measurement in Fig. 4 for hyperspectral image. The spectra for HLB1, HLB2, and Healthy are the average of 49, 20, and 11 pixel spectra, respectively. (b) Spectral plot of PCR test confirmed HLB infected and Healthy tree pixels in hyperspectral and multispectral images. Each spectrum is an average of 15 observation points.

The PCR test confirmed HLB and Healthy trees from the image sites. The trees corresponding to this ground truthing data were located, and their pixel spectra were plotted for both hyperspectral and multispectral images, shown in Fig. 5(b). Figure 5(b) shows a higher DN value for HLB infected pixels corresponding to their Healthy counterpart. This result is again consistent with the reflectance measurements using a handheld spectrometer at the grove site. Figure 6 shows that the ratio of HLB infected spectrum to healthy spectrum [of Figs. 4(a), 5(a), and 5(b)] is almost always greater than 1.

5.3 HLB Infected Pixel Detection Using MTF

Figure 7 shows the results from MTF¹⁸ with an MNF¹⁹⁻²¹ image. From the validation set of images taken in 2007, minimum noise fraction (MNF) transform was applied to a spectrally subset reflectance image [Fig. 7(a)], and then the MNF eigenvalue plot was analyzed. After

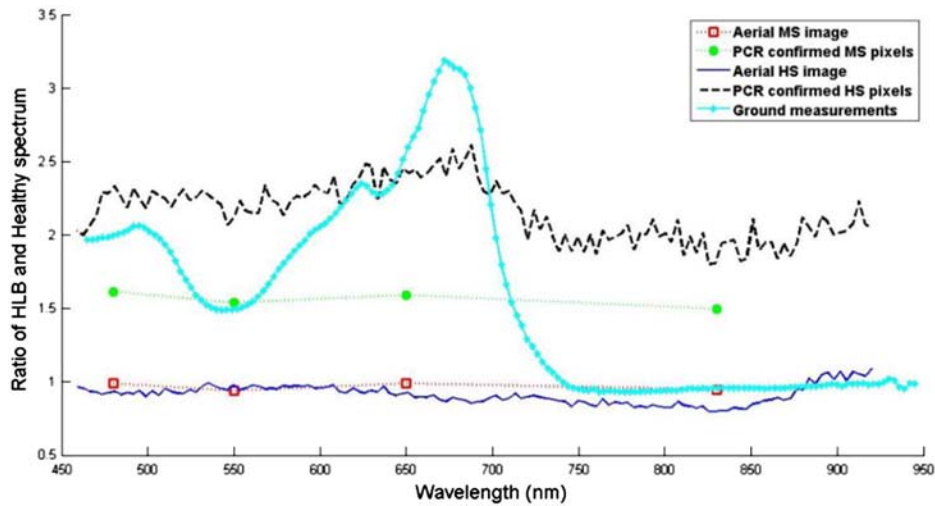


Fig. 6 Ratio of HLB to Healthy spectrum of Figs. 4(a), 5(a), and 5(b).

the pixel purity index (PPI) function was run on the MNF transform result [Fig. 7(b)], the purest pixels were clustered [Fig. 7(c)] using the n-D visualizer tool with MNF data that used only the purest pixels. The purest pixels were saved as a library of pure endmember collection. Then, three classes of pure endmembers for the vegetation, dark shadow pixels, and soil pixels were obtained from the scatter plot [Fig. 7(c)]. Figure 7(d) shows the pure endmember pixels projected as regions of interest indicating vegetation (green), soil (brown), and shadow (magenta) pixels. The shadow and soil pixels were used to create a mask band for MTMF. The output contains a

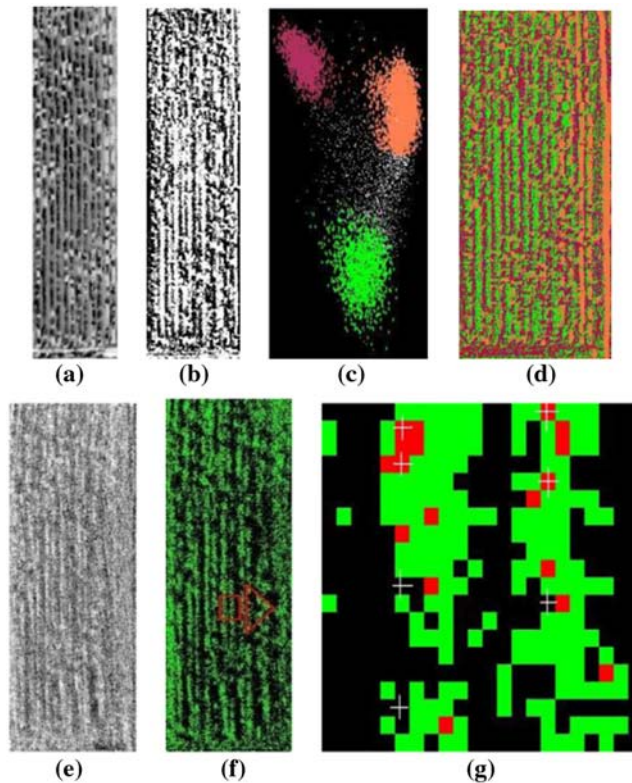


Fig. 7 MTMF applied on a large tree section image from 2007 set: (a) MNF transformed hyperspectral image, (b) PPI image, (c) pure endmembers selected in n-D scatter plot, (d) pure endmember pixels projected as regions of interest indicating vegetation (green), soil (brown), and shadow (magenta) pixels, (e) MF score image, (f) Rule classifier threshold image based on score and infeasibility, and (g) enlarged subsection of a red box in figure (f).

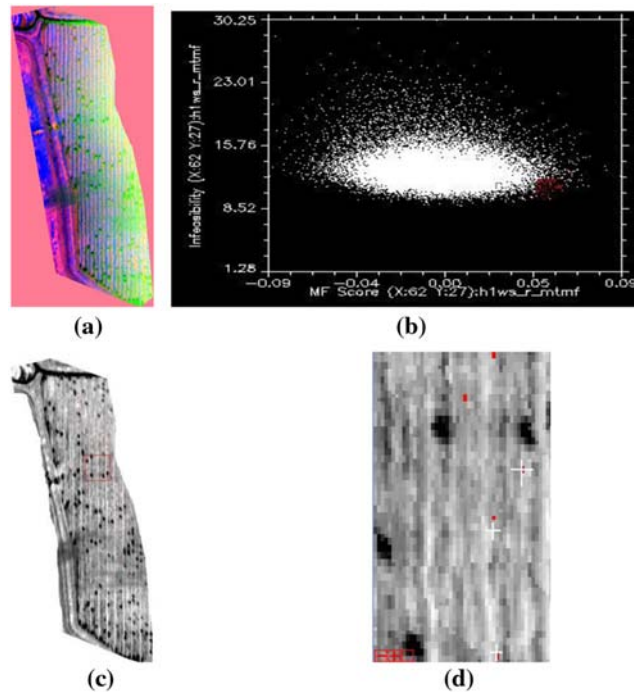


Fig. 8 MTMF method applied on E1 (west grove site): (a) MNF RGB image (retains all spectrally pure pixels), (b) 2D scatter plot of pixels after MTMF is carried out on (a). A low infeasibility and high MF score indicated a better match to the endmember spectra (HLB pixels) being detected. These pixels have the color red in the scatter plot, (c) target endmember (HLB pixels) projected on the MTMF output image as red pixels, (d) the white cross-hair on the enlarged rectangular subsection of (c) indicates ground truth location for infected trees.

matched filter (MF) score image and an infeasibility image corresponding to each MNF band. Pixels with high MF score and low infeasibility value indicated a better match to the reference spectra. It was observed that the PPI masked many of the canopy edge pixels, which was due to the canopy edge pixels being darker than the rest of the vegetation. These processing steps were conducted first to filter out nonvegetation pixels from the image, and then to identify HLB infected pixels based on MF score and infeasibility. Figure 7(f) and 7(g) shows the final detection results in which crosshairs are ground truthing locations of infected tree canopies and red pixels are the identified pixels by the algorithm. Figure 7(g) shows six correctly identified HLB infected trees.

The same method was applied to the hyperspectral images for the east and west grove sites (E1) in the 2009 images. The MNF transform was applied to the raw image data to create MNF bands. This segregated valuable spectral information and undesirable noise. Lower MNF bands contain most of the spectral information, and higher MNF bands can be discarded, as they contain most of the image data noise. The existing image derived spectral library for hyperspectral images was used by the MTMF on the MNF transformed image to match the HLB infected endmember spectra as shown in Figs. 8 and 9.

Let us consider the set $MTMF_HLB$ as the collection of pixels detected as HLB infected and PCR_HLB as the set of all PCR confirmed HLB pixels within the site. The intersection of the sets PCR_HLB and $MTMF_HLB$, i.e., $MTMF_PCR_HLB$ would be an estimate of the accuracy of the MTMF detection method. Table 5 estimates the detection accuracy of MTMF analysis results. Pixels detected as infected are validated against the PCR confirmed ground truthing data.

5.4 HLB Diseased Pixel Detection Using Spectral Angle Mapping

Figure 10 shows an example procedure for disease detection using the SAM. A reflectance image from the 2007 validation set images was converted to NDVI image to generate a new image with only tree canopy pixels. SAM analysis used the existing image derived spectral

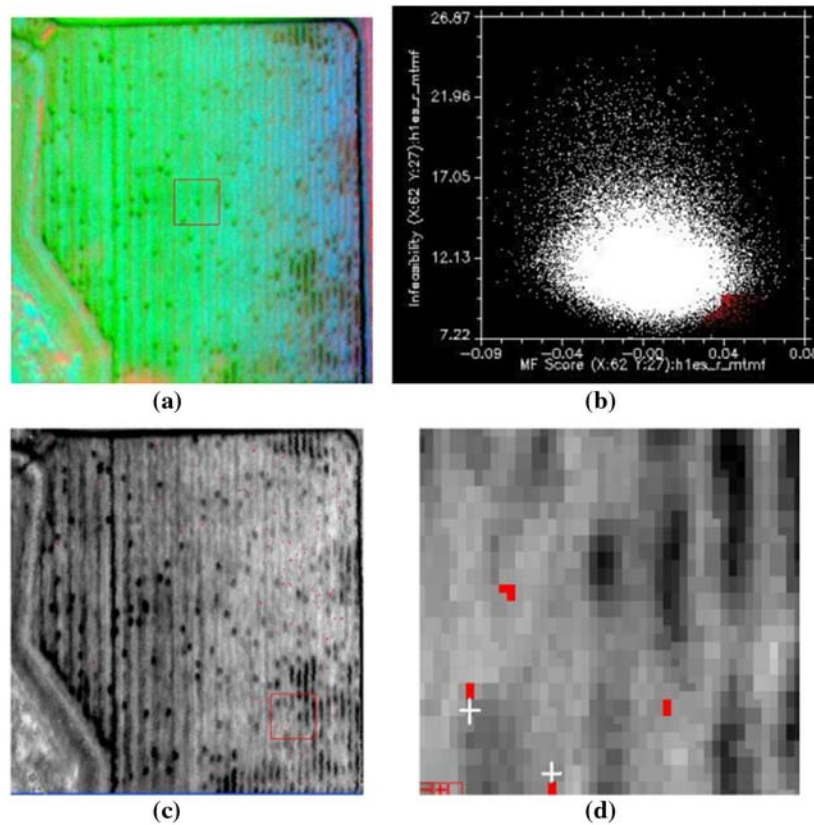


Fig. 9 MTMF method applied on E1 (east grove site): (a) MNF RGB image which retains all spectrally pure pixels, (b) 2D scatter plot of pixels after MTMF is carried out on (a). A low infeasibility and high MF score indicated a better match to the endmember spectra (HLB pixels) being detected. These pixels have the color red in the scatter plot, (c) target endmember (HLB pixels) projected on the MTMF output image as red pixels, (d) the white cross-hairs inside the red box of (c) indicate ground truth location for infected trees.

libraries using 300 pixels each for both categories (Healthy and HLB infected). Multiple maximum spectral angles were used for the SAM algorithm for mapping pixels. A spectral angle of 0.1 radians was used for the entire endmember collection of healthy pixels, and an angle of 0.08 radians for the diseased pixel endmembers gave optimum results for the young tree section. Table 6 displays the consolidated SAM results. The results were verified with the ground truth data, and the accuracies ranged from 32% to 65%.

The occurrence of false positives confirms the misclassification observed during the discriminant analysis, as there were more false positives in the large tree sections than in the young tree sections. One of the potential sources of error in the identification process is the inaccuracy of the ground truthing. A GPS positioning error of one to three meters while recording positions would result in a shift of one to four pixels, leading to corruption of the endmember image derived spectral library created for the analysis. Therefore, a buffer of 9×9 pixels with a ground truth location at the center was used to take this pixel error into account. By including a buffer of four pixels in all directions from the ground truth point, infected trees were identified with a much better accuracy. The inaccuracy of four pixels corresponds to an estimated error of maximum three meters in the ground truth. Accuracies of 72% and 76% were obtained for large and

Table 5 MTMF accuracy of the 2009 validation hyperspectral image.

Site	Imagetype	PCR_HLB (pixels)	MTMF_PCR_HLB (pixels)	Accuracy (%)
E1–West	HS	15	11	73.3
E1–East	HS	15	12	80.0

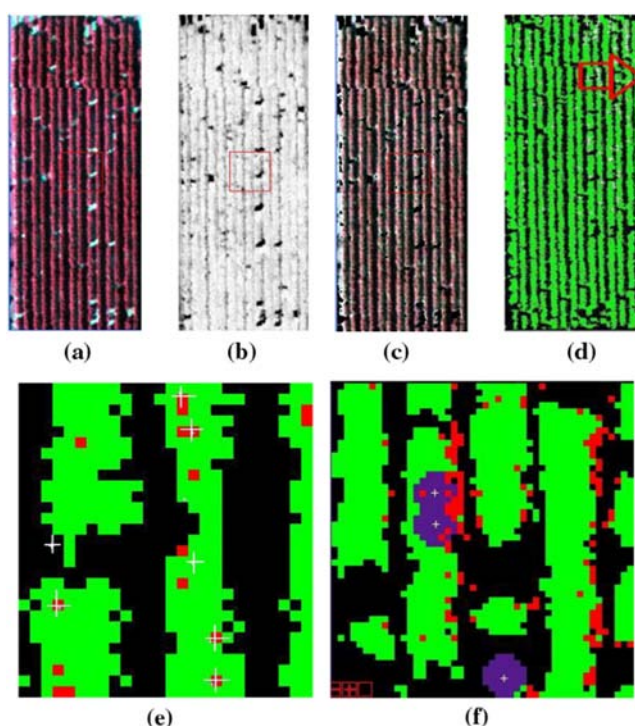


Fig. 10 SAM procedure applied on a large-tree section: (a) original hyperspectral image, (b) corresponding NDVI image, (c) mask image created using NDVI threshold, (d) SAM result of the image, (e) Enlarged red box in (d). Green pixel is healthy vegetation, and red pixel was identified as HLB infected pixels. The white cross-hair indicates ground truth location for infected trees. (f) Classification using a buffer. The purple region around the white plus signs is the buffer region.

young trees, respectively (Table 6). In Fig. 10(f), the purple discs around the white pluses denote the buffer region. Any red pixels within this region count as a correct identification. For example, the two infections at the center were identified, but the one at the bottom was not, because the red pixels are just outside the purple region.

The identification results are heavily dependent on the quality of the endmember spectra collected, which in turn depends on the accuracy of the ground truth data. Thus, ground truthing should be done with a more accurate GPS receiver such as an RTK GPS receiver. This would definitely yield better results.

The SAM analysis for the images in 2009 used the existing image derived spectral library created from 30 pixels each for both categories (Healthy and HLB infected), confirmed using PCR tests. Multiple maximum spectral angles were used for the SAM algorithm for mapping pixels. A spectral angle of 0.1 radians was used for the entire endmember collection of healthy pixels. An angle of 0.05 radians was used for the diseased pixel endmembers, and it was found to give optimum results for both E1 sites in the hyperspectral image. Figure 11 documents the steps involved in the SAM analysis.

Table 6 SAM analysis results on the 2007 images from the validation set for both Large and Young tree sections and its accuracy based on comparison with ground truthing data.

Tree size	No. of infected pixels by ground truthing	Without buffer		With buffer	
		No. of pixels correctly identified by SAM	Accuracy (%)	No. of pixels correctly identified by SAM	Accuracy (%)
LARGE	290	166	57.2	210	72.4
YOUNG	142	66	46.4	108	76.0

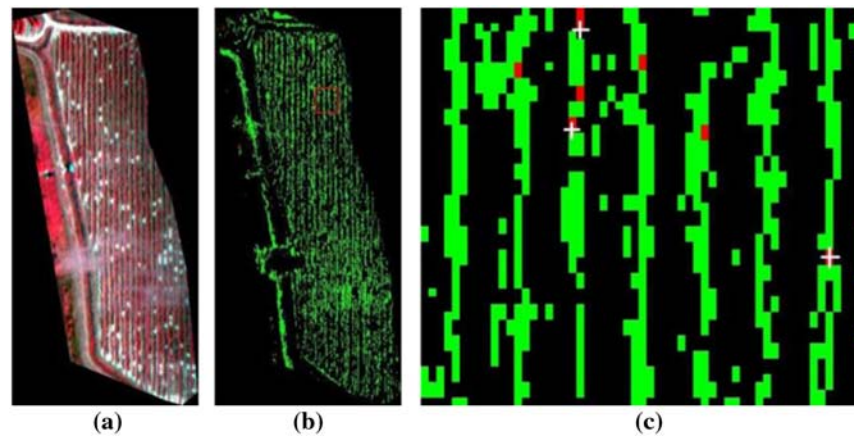


Fig. 11 SAM procedure applied on E1 (west grove site): (a) original hyperspectral color infrared (CIR) image, (b) SAM result. Green pixel is healthy vegetation, and red pixel was identified as HLB infected pixels, (c) zoomed-in picture of the red square in (b). The white cross-hair indicates ground truth location for infected trees.

The corresponding spectral library for multispectral images was used while carrying out the SAM analysis on both multispectral image sites. A spectral angle of 0.1 radians was used for the entire endmember collection of healthy pixels, and an angle of 0.04 radians was used for the diseased pixel endmembers. This was found to yield optimum results for both E1 sites in the multispectral image.

Let us consider the set SAM_HLB as the collection of pixels detected as HLB infected and PCR_HLB as the set of all PCR confirmed HLB pixels within the site. The intersection of these two sets, SAM_PCR_HLB, would be an estimate of the accuracy of the SAM detection method. Table 7 estimates the detection accuracy of SAM analysis results. Pixels detected as infected were validated against the PCR confirmed ground truthing data.

It can be seen from Table 7 that the multispectral images resulted in a better accuracy than the hyperspectral images. The 2009 images also led to a better performance than the 2007 images owing to positioning errors for the 2007 images. The multispectral images yielded better results than the hyperspectral images. While hyperspectral images indeed contain a lot more information than multispectral images, the increased dimensionality and redundant information in adjacent bands of the hyperspectral image sometimes lead to lower accuracy values. Such instances have been seen in other studies as well, with either no significant improvements were observed for hyperspectral imagery,²² or individual accuracies for particular classes was higher,²³ or the overall accuracy itself was greater.²⁴

The increase in HLB identification efficiency with a buffer is expected, and similar results were observed for the 2009 images as well. Section 5.7 discusses the case where the buffer spans the canopy of the corresponding tree ('tree-based' classification). Similar increase in accuracy was observed.

Table 7 SAM accuracy for the 2009 imagery. HS and MS stand for hyperspectral and multispectral images, respectively.

Site	Imagetype	PCR_HLB (pixels)	SAM_PCR_HLB (pixels)	Accuracy (%)
E1-West	HS	15	9	60.0
E1-East	HS	15	10	66.6
E1-West	MS	15	12	80.0
E1-East	MS	15	13	86.6

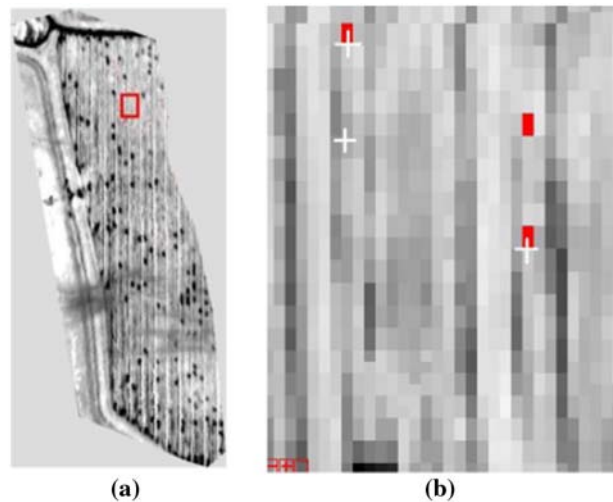


Fig. 12 Spectral unmixing method applied to E1 (west grove site): (a) spectral unmixing applied on MNF transformed image of Fig. 8(a). Red pixels indicate infected trees which were matched based on high abundance threshold value. (b) The white cross-hair on the enlarged rectangular subsection of figure (a) indicates ground truth location for infected trees.

5.5 HLB Diseased Pixel Detection Using Linear Spectral Unmixing

This analysis was carried out only on the validation image set of 2009. The spectral unmixing method was applied on both the hyperspectral images for the east and west grove site (E1). The MNF transform was applied to the raw image data to create MNF bands to obtain spectrally pure pixels. Spectral unmixing procedure was applied to the MNF data. This technique found the abundance of the endmember spectra (HLB infected pixels provided as input using the spectral library) in each reference spectra of the MNF image. Detection of HLB infected pixels was achieved using a high threshold on the abundance value of the unmixed output pixels, indicating a better match to endmember spectra as shown in Fig. 12.

Let us consider the set LSU_HLB as the collection of pixels detected as HLB infected. The intersection of the sets LSU_HLB and PCR_HLB, i.e., LSU_PCR_HLB, would be an estimate of the accuracy of the LSU detection method. Table 8 estimates the detection accuracy of LSU analysis results. Pixels detected as infected are validated against the PCR confirmed ground truthing data. The result of the LSU method applied to E1 grove is shown in Fig. 13.

It was seen that the E1-west site accuracy was lower than the east site for all the above methods. The E1-west site consisted of 32 rows of trees, out of which only 12 tree rows could be used for hyperspectral data processing. The other parts of the image were unavailable due to poor quality and interference of cloud clusters.

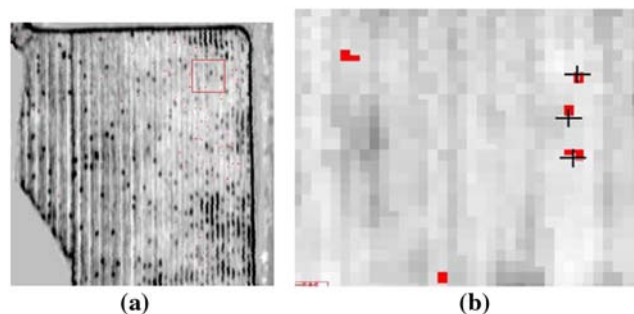


Fig. 13 Linear Spectral Unmixing method applied to E1 (east grove site): (a) Spectral unmixing applied on MNF transformed image of Fig. 9(a). Red pixels indicate infected trees which were matched based on high abundance threshold value, (b) The black cross-hair on the enlarged rectangular subsection of figure (a) indicates ground truth location for infected trees.

Table 8 Linear spectral unmixing (LSU) accuracy for the 2009 validation set images.

Site	Imagetype	PCR_HLB (pixels)	LSU_PCR_HLB (pixels)	Accuracy (%)
E1-West	HS	15	8	53.3
E1-East	HS	15	11	73.3

Table 9 Pixel-based validation of the image after applying false positive reduction.

IMAGEBlock 2 Section4	Number of healthy pixels	Number of HLB pixels	TOTAL
HEALTHY	94,512	88	94,600
HLB	16	7 (30.0%)	23

Table 10 Tree-based validation of the image after applying false positive reduction.

IMAGEBlock 2 Section4	Number of healthy trees	Number of HLB trees	TOTAL
HEALTHY	94,512	88	94,600
HLB	8	15 (65.2%)	23

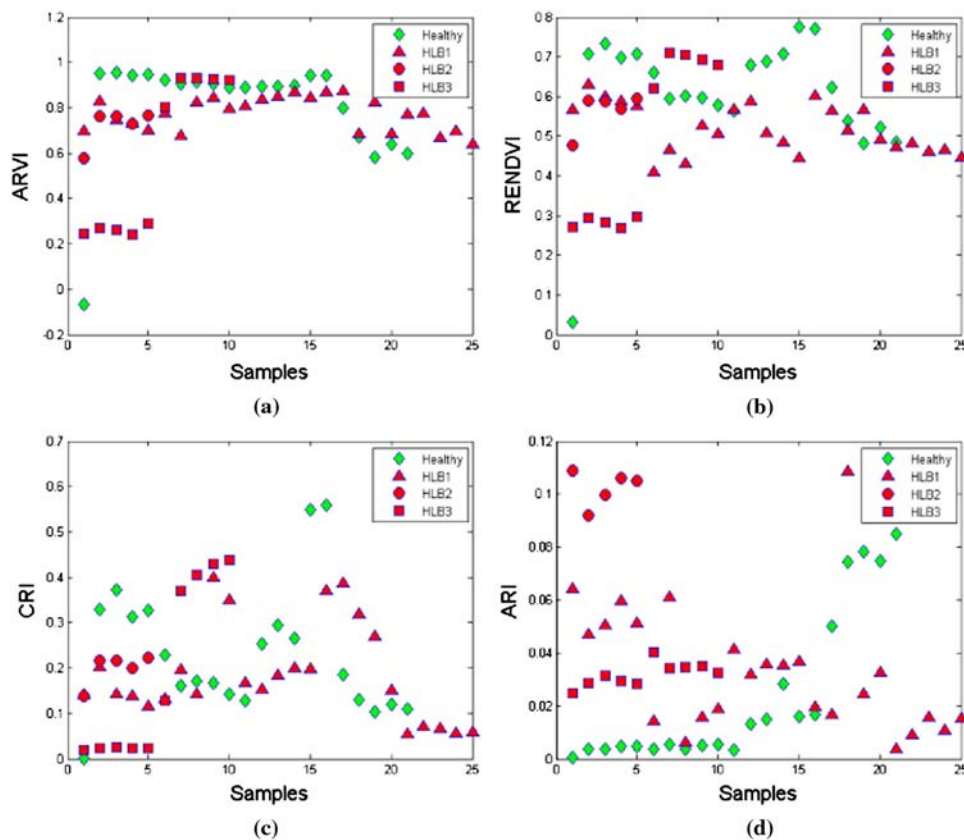


Fig. 14 Vegetation indices and leaf pigment indices calculated on ground observations: (a) atmosphere resistant vegetation index, (b) red edge NDVI, (c) carotenoid reflectance index, and (d) anthocyanin reflectance index.

As a result, ground information and PCR results of only the first 12 rows could be utilized in the spectral library construction. This could explain the variation in the accuracy results in the west and east grove sites. The accuracy results were strictly based on the intersection of the two sets, the PCR_HLB and the set of all trees detected as infected by the detection method. The PCR results are not available for every tree in the grove, as conducting such a comprehensive test on the grove site would be extremely time-consuming and costly. Having more positive PCR results increases the size of the set PCR_HLB which would provide a better estimate of the accuracy, since the intersection of the two sets is bound to increase or decrease based on the performance of the method.

Since the status of every tree on the grove was not known, quantizing the false positives (healthy tree identified as infected) was not possible. This would have provided an even better representation and accuracy of the results.

5.6 Reduction of False Positives from Results: 2007 Images

A false positive pixel collection of 30 samples was built from the validation set using the image results obtained from the SAM image analysis. ANOVA was carried out on the reflectance data obtained from the false positive samples and HLB pixel collection to extract bands which could separate the two categories. Based on the ANOVA results, 11 significant bands were extracted, which could separate the two categories of 'true HLB' and 'false HLB' (false positives). Those identified spectral bands were 864.45, 874.11 to 888.61, 898.28, 903.11, 912.79 to 922.50, and 975.88 nm. The SAM method was applied to a selected image using the above spectral library. The detection accuracy was calculated using two approaches, i.e., a pixel-based (Table 9) and a tree-based validation approach (Table 10). The tree-based approach was adapted for a more

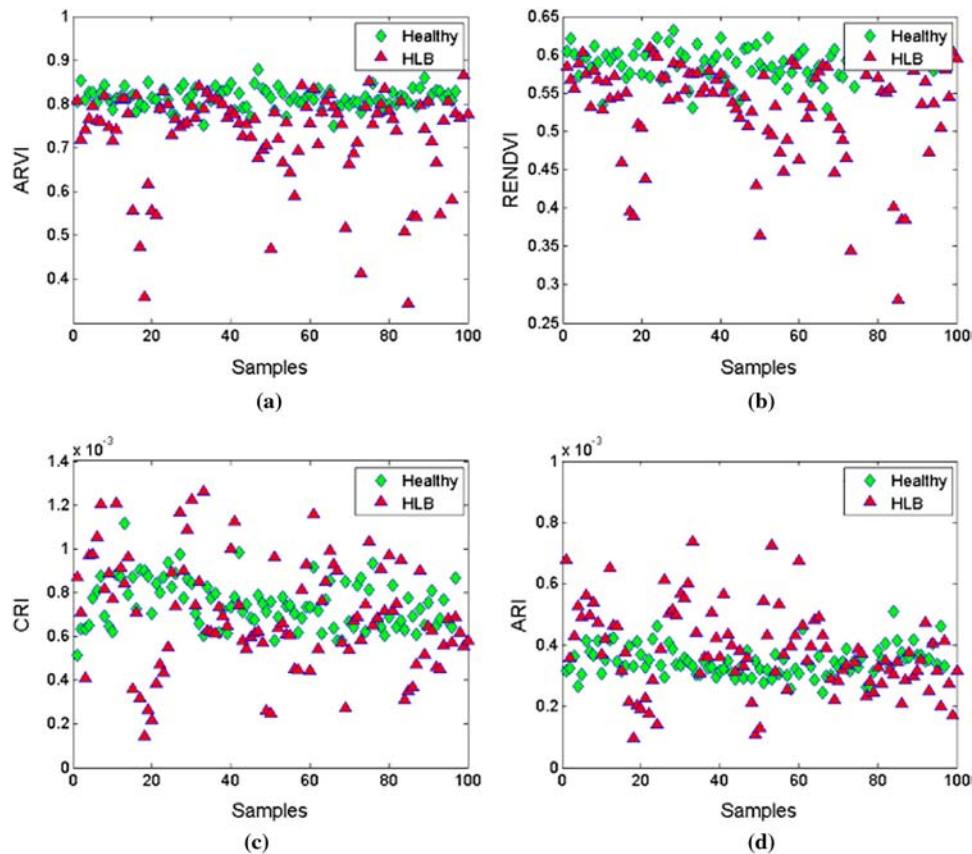


Fig. 15 Vegetation indices and leaf pigment indices calculated from the spectral library: (a) atmosphere resistant vegetation index, (b) red edge NDVI, (c) carotenoid reflectance index, and (d) anthocyanin reflectance index.

Table 11 SAM results using the spectral library refined by the VI results.

IMAGEBlock 2 Section4	Number of healthy pixels	Number of HLB pixels	TOTAL
HEALTHY	94,524	76	94,600
HLB	5	18 (78.6%)	23

realistic documentation of the accuracy of the results, since a tree is determined to be infected if its canopy (pixels) is infected. With the tree-based detection, the detection accuracy increased from 30% to 65% for a given image, as shown in Tables 7 and 8.

5.7 Improving Spectral Library Using Vegetation and Leaf Pigment Indices

The chosen VIs and leaf pigment indices were calculated using observations from ground measurements and spectral library for each of the categories of HLB infected and healthy trees. The results of the VIs for the various samples (Figs. 14 and 15) and their magnitude range for different categories were observed. The vegetation indices and leaf pigment indices were able to separate the Healthy and the HLB infected observation points.

Based on the above indices, thresholds for each index between Healthy and HLB pixels were determined and then used to refine the spectral library, which eventually contained only true HLB pixels and true Healthy pixels. Because DN was used to calculate the indices rather than the reflectance, the value of the different indices is different from the expected range of values.

ANOVA was carried out on the refined spectral library. Based on the p -value in the ANOVA with a 95% significance level, 28 significant bands were extracted and a new spectral library was constructed using these bands. Table 11 shows the SAM results using the above spectral library. When the results were compared between Tables 8 and 9, the detection accuracy increased from 65.2% to 78.6%, indicating the great potential of utilizing the vegetation and leaf pigment indices in order to refine the results of the other methods such as SAM.

6 Conclusion

Hyperspectral imagery, observations from ground measurements, image derived spectral library, MTMF, spectral angle mapping (SAM), and LSU methods in the imaging software (ENVI) were used to detect areas of HLB infection. For the images from 2007, the n-D scatter plot used for the MTMF analysis indicated that not all pixels were identified as a part of a pure endmember class. Not all vegetation pixels were spectrally pure, and pixel values varied from the left side to the right side of a tree row across a canopy. Moreover, due to the similarity in the spectra of Healthy and HLB infected tree pixels at the canopy edge, results from the MTMF and SAM analyses yielded false positives, i.e., healthy pixels identified as infected. An overall accuracy of approximately 60% was observed using SAM. There is a clear possibility of inaccuracy of ground truthing data because of geo-referencing error. Moreover, the airborne hyperspectral images only guaranteed a position accuracy of one to two pixels. Better atmospheric correction methods for taking care of illumination variance and normalization of canopy edge pixels would help in yielding better results. More accurate ground truth information would further help in validating the results.

For the site selected in 2009, polymerase chain reaction (PCR) test-based ground truthing of selected trees in the area had been carried out to determine the status of these trees and classifying them into healthy or infected. These observations were used for spectral library construction as well as validation and accuracy estimation of the results. Ground measurements with a handheld spectrometer were also obtained for Healthy and HLB infected citrus trees from the same grove site along with their degrees of infection. This was used as an alternative to PCR results for result validation. A fairly high detection accuracy of 80% was achieved using MTMF on hyperspectral image of the E1-east site. SAM with multispectral images also gave a very high accuracy

rate of 87%. The E1-west site observed lower detection accuracy compared to the east site. This was due to the fact that the hyperspectral image was cropped due to poor quality, and hence all ground measurements for this site could not be utilized, as all tree rows were not available for hyperspectral image processing. The multispectral images yielded better detection results than the hyperspectral images. A better estimate of accuracy can be achieved with more PCR results and a more comprehensive ground survey. This would help in the quantization of false positives in the results.

Acknowledgments

The authors would like to thank Mr. Ashish Mishra, Ms. Sherrie Buchanon, Ms. Ujwala Jadhav, and Mr. Eduardo Chica at the CREC in the University of Florida, Mr. Anurag Katti in the Electrical and Computer Engineering in the University of Florida, Dr. Eran Raveh at the Agricultural Research Organization, Israel, and Mr. James Colee, UF/IFAS statistical consultant, for their assistance. We also thank Mr. Michael Ohlinger of Sterling Air Service at Weslaco, TX, and Mr. Fred Gomez of USDA-ARS at Weslaco, TX, for taking the multispectral and hyperspectral imagery in 2009 and Mr. Jim Forward of USDA-ARS at Weslaco, TX, for preprocessing the imagery. This project was funded by the Citrus Research and Development Foundation, Inc.

References

1. M. Garnier et al., "Genomic characterization of a *Liberibacter* present in an ornamental rutaceous tree, *Calodendrum capense*, in the Western Cape province of South Africa. Proposal of 'Candidatus *Liberibacter africanus* subsp. *capensis*,'" *Int. J. Syst. Evol. Microbiol.* **50**(6), 2119–2125 (2000), <http://dx.doi.org/10.1099/00207713-50-6-2119>.
2. FDACS DPI, "Huanglongbing (HLB)/citrus greening disease," 2006, <http://www.doacs.state.fl.us/pi/chrp/greening/citrusgreening.html> (7 September 2006).
3. R. H. Brlansky, K. R. Chung, and M. E. Rogers, "2006 Florida citrus pest management guide: Huanglongbing (citrus greening)," UF/IFAS Extension (2012).
4. FDACS DPI, "Disease detection maps: Known distribution of citrus canker/citrus greening (HLB) in Florida," (2010), <http://www.doacs.state.fl.us/pi/chrp/ArcReader/ArcReader.html> (6 April 2010).
5. Y. Tian, S. Ke, and C. Ke, "Polymerase chain reaction for detection and quantization of *Liberobacter asiaticum*, the bacterium associated with Huanglongbing (Greening) of citrus in China," in *Proc. 13th Conference of the International Organization of Citrus Virologists (IOCV)*, pp. 252–257, University of California, Riverside, USA (1996).
6. A. Morris and R. Muraro, "Economic evaluation of citrus greening management and control strategies," UF/IFAS EDIS Publication FE712 (2008).
7. J. Qin et al., "Detection of citrus canker using hyperspectral reflectance imaging with spectral information divergence," *J. Food Eng.* **93**(2), 183–191 (2009), <http://dx.doi.org/10.1016/j.jfoodeng.2009.01.014>.
8. C. Yang, "Assessment of the severity of bacterial leaf blight in rice using canopy hyperspectral reflectance," *Precis. Agr.* **11**(1), 61–81 (2010). <http://dx.doi.org/10.1007/s11119-009-9122-4>
9. K. Matsuo et al., "Development of experimental setup for distinction of disease plant," ASABE Paper No. 063016, St. Joseph, Mich.: ASABE (2006).
10. K. Lee et al., "Hyperspectral imaging for detecting defect on apples," ASAE Paper No. 053075. St. Joseph, Mich.: ASABE (2005).
11. C. Yang, "An airborne four-camera imaging system for agricultural applications," ASABE Paper No. 1008855, St. Joseph, Mich.: ASABE (2010).
12. C. Yang et al., "A CCD camera-based hyperspectral imaging system for stationary and airborne applications," *Geocarto Int. J.* **18**(2), 71–80 (2003), <http://dx.doi.org/10.1080/10106040308542274>.
13. J. W. Rouse et al., "Monitoring vegetation systems in the Great Plains with ERTS," *Third ERTS Symposium, NASA SP-351*, Greenbelt, MD, 309–317 (1973).

14. F. A. Kruse et al., "The spectral image processing system (SIPS)—interactive visualization and analysis of imaging spectrometer data," *Rem. Sens. Environ.* **44**, 145–163 (1993), [http://dx.doi.org/10.1016/0034-4257\(93\)90013-N](http://dx.doi.org/10.1016/0034-4257(93)90013-N).
15. A. A. Gitelson and M. N. Merzlyak, "Spectral reflectance changes associated with autumn senescence of *Aesculus hippocastanum* L. and *Acer Platanoides* L. leaves. Spectral features and relation to chlorophyll estimation," *J. Plant Physiol.* **143**, 286–292 (1994), [http://dx.doi.org/10.1016/S0176-1617\(11\)81633-0](http://dx.doi.org/10.1016/S0176-1617(11)81633-0).
16. Y. J. Kaufman and D. Tanre, "Strategy for direct and indirect methods for correcting the aerosol effect on remote sensing: from AVHRR to EOS-MODIS," *Rem. Sens. Environ.* **55**, 65–79 (1996), [http://dx.doi.org/10.1016/0034-4257\(95\)00193-X](http://dx.doi.org/10.1016/0034-4257(95)00193-X).
17. G. P. Asner, "Biophysical and biochemical sources of variability in canopy reflectance," *Rem. Sens. Environ.* **64**, 234–253 (1998), [http://dx.doi.org/10.1016/S0034-4257\(98\)00014-5](http://dx.doi.org/10.1016/S0034-4257(98)00014-5).
18. J. W. Boardman, "Leveraging the high dimensionality of AVIRIS data for improved sub-pixel target unmixing and rejection of false positives: Mixture Tuned Matched Filtering," in *Proc. 7th Annual JPL Airborne Geoscience Workshop*, JPL Publication 97-1, Pasadena, CA, p. 55 (1998).
19. A. A. Green et al., "A transformation for ordering multispectral data in terms of image quality with implications for noise removal," *IEEE Trans. Geosci. Rem. Sens.* **26**, 65–74 (1988), <http://dx.doi.org/10.1109/36.3001>.
20. J. W. Boardman and F. A. Kruse, "Automated spectral analysis: a geological example using AVIRIS data, north Grapevine Mountains, Nevada," in *Proc. ERIM Tenth Thematic Conference on Geologic Remote Sensing*, p. I-407, Environmental Research Institute of Michigan, Ann Arbor, MI (1994).
21. R. N. Clark and T. L. Roush, "Reflectance spectroscopy: quantitative analysis techniques for remote sensing applications," *J. Geophys. Res.* **89**, 6329–6340 (1984), <http://dx.doi.org/10.1029/JB089iB07p06329>.
22. C. Yang, J. H. Everitt, and C. J. Fernandez, "Comparison of airborne multispectral and hyperspectral imagery for mapping cotton root rot," *Biosystems Eng.* **107**, 131–139 (2010), <http://dx.doi.org/10.1016/j.biosystemseng.2010.07.011>.
23. K. T. Weber et al., "A comparison between multi-spectral and hyperspectral platforms for early detection of leafy spurge in southeastern Idaho," in *Final report: Detection, prediction, impact, and management of invasive plants using GIS*, K. T. Weber, Ed., pp. 186–196, NASA, Greenbelt, MD (2006).
24. S. Taylor, L. Kumar, and N. Reid, "Comparison of Broadband and Hyperspectral Sensors for Lantana Mapping," in *Proc. 34th International Symposium on Remote Sensing of Environment*, Sydney, Australia, (2011).



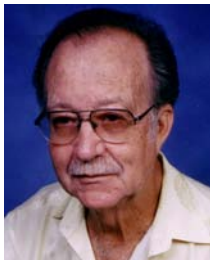
Arun Kumar has worked as a design engineer at LSI Corp. and an R&D engineer at Synopsys Inc. He received his BS degree in computer science and engineering from Govt. Engineering College, Thrissur, Kerala, India and a MS in electrical and computer engineering from University of Florida, Gainesville, FL, USA. His current interests are in the area of hyperspectral image processing using field programmable gate arrays (FPGA).



Won Suk Lee is currently is an associate professor in the Agricultural and Biological Engineering Department in the University of Florida. He received his BS and MS degrees in agricultural engineering from the Seoul National University in Korea in 1986 and 1988, respectively, and a PhD degree in biological and agricultural engineering from the University of California, Davis in 1998. His research interests focus on developing sensing systems for precision agriculture and farm automation.



Reza Ehsani received his PhD in biological and agricultural engineering from the University of California, Davis in 2000, where he worked on precision agriculture applications for high value crops. Currently, he is an associate professor of agricultural and biological engineering at the University of Florida/IFAS Citrus Research and Education Center (CREC). His current areas of research include developing tools and techniques for precision horticulture management, applications of low-cost unmanned flying platform for orchard management and precision horticulture, optical sensors for stress detection, and automation and machine enhancement for citrus mechanical harvesters.



L. Gene Albrigo is a professor in the Horticulture Department at the Citrus Research and Education Center in the University of Florida. He received his BS degree in pomology in 1962 and MS degree in plant physiology in 1964 both from the University of California, Davis, and a PhD degree in horticulture from the Rutgers University in 1968. He has served as the President of the International Society of Citriculture in 1996 to 2000 and is a fellow of the American Society of Horticultural Science.



Chenghai Yang is an agricultural engineer with the USDA-Agricultural Research Service's Southern Plains Agricultural Research Center in College Station, Texas. Prior to that, he was an agricultural engineer at the USDA-ARS Kika de la Garza Agricultural Research Center in Weslaco, Texas from 1995 to 2012. He received his BS and MS degrees in agricultural engineering from Northwest A&F University in China, and his PhD degree in agricultural engineering from the University of Idaho in 1994. His research has been focused on the use of remote sensing and other spatial information technologies for precision agriculture and pest management.



Robert L. Mangan has conducted research concerning evolution, reproduction, and population ecology of insects since 1968. His doctoral training was concerned with ecological and genetic factors determining host plant selection in Diptera. Since 1982 his research has focused on behavior, population ecology, and genetics of pest populations in support of eradication programs. He served as research leader and conducted research with the USDA ARS Crop Quality and Fruit Insects Research unit in Weslaco, Texas from 1989 until 2012 when he assumed the position as research leader and location director at the Subtropical Horticultural Research Station at Miami Florida.